Journal of Electroanalytical Chemistry 799 (2017) 102–110

Contents lists available at ScienceDirect

Journal of Electroanalytical Chemistry

journal homepage: www.elsevier.com/locate/jelechem

RGO/$ZnWO_4$/Fe_3O_4 nanocomposite as an efficient electrocatalyst for oxygen reduction reaction

M. Mohamed Jaffer Sadiq[a], Sankararao Mutyala[b], Jayaraman Mathiyarasu[b], D. Krishna Bhat[a,*]

[a] Department of Chemistry, National Institute of Technology Karnataka, Surathkal, Mangalore 575025, India
[b] Electrodics and Electrocatalysis Division, CSIR-Central Electrochemical Research Institute, Karaikudi 630003, India

ARTICLE INFO

Keywords:
RGO/$ZnWO_4$/Fe_3O_4 catalyst
Oxygen reduction reaction
Electrocatalyst
Microwave irradiation
Fuel cell

ABSTRACT

Development of low cost, environmental friendly and noble metal free catalyst materials with excellent performance is essential for commercialization. In fact, this is the need of the day too. Herein, we report a facile microwave irradiation method for the synthesis of novel RGO/$ZnWO_4$/Fe_3O_4 cathode catalysts for the oxygen reduction reaction (ORR) in alkaline medium. The structural and morphological features of synthesized materials are fully examined using transmission electron microscopy (TEM), high resolution transmission electron microscopy (HRTEM). The chemical composition and elemental analysis of the catalyst is investigated by X-ray diffraction (XRD), X-ray photoelectron spectroscopy (XPS) and Raman spectroscopy techniques. Efficiency of RGO/$ZnWO_4$/Fe_3O_4 catalyst material for oxygen reduction reaction (ORR) in 0.1 M KOH is reported. The activity of catalyst is determined by linear sweep voltammogram (LSV) and rotating disk electrode (RDE) measurements in O_2 saturated 0.1 M KOH electrolyte. RGO/$ZnWO_4$/Fe_3O_4 catalyst exhibits higher ORR activity than RGO, $ZnWO_4$, RGO/$ZnWO_4$ and its electrocatalytic performance is comparable to Pt/C material and is superior to it in stability and methanol tolerance. Further, it is determined that process follows a direct four electron reaction pathway. These combined results strongly signpost that RGO/$ZnWO_4$/Fe_3O_4 composite can function as an economic noble metal free ORR cathode catalyst for energy applications.

1. Introduction

In this era of energy crisis and global warming, development of technologies to create safe, cost effective, green, sustainable and highly efficient energy resources have become crucial [1]. Fuel cell technology is one of the best alternative energy sources which can convert chemical energy into electrical energy because it has high power density and is free from pollution [1]. Electrocatalyst for ORR is crucial in adjusting the performance of fuel cells and metal air batteries because ORR is lethargic in nature [2–4]. The existing platinum based materials are highly efficient ORR catalysts for the commercial fuel cells. However, high cost, less durability and intolerance to the crossover effect makes it difficult to be used for mass production [5]. Hence developing various nonprecious metal free electrocatalysts with cheap and high activity for ORR have been regarded as a great challenge in the field of fuel cells [3,6].

Recently, emerging platinum-free electrocatalysts for ORR including carbon materials, transition metal oxides, and metal chalcogenides have gained enormous interest in the scientific community. Especially, carbon materials have been a promising noble metal-free electrocatalysts for ORR, because of a large number of active sites and high conductivity. Carbon based materials such as carbon nanotube and graphene are unique candidates for electrochemical applications in supercapacitors, sensors, catalysts, and fuel cells etc. [7–10]. Graphene, a single layer of carbon atoms, covalently bonded into a hexagonal lattice, is suitable for electrochemical processes because of its excellent electrical properties and theoretically ultrahigh specific surface area [11,12]. The addition of certain transition metals or metal oxides to the graphene materials can improve the ORR activity compared to the benchmark platinum catalyst due to synergistic effect between metal and carbon materials [6,13,14].

In this respect, a broad range of an alternative catalyst based on non-precious metals or metal oxides such as, Fe, Co, Fe_2O_3, Fe_3O_4, Co_3O_4, NiO and ZnO have been considered in the past [6,13–16]. Among these potential materials, Fe_3O_4 can be used as a potential ORR catalyst for alkaline fuel cells due to its high efficiency, low cost, eco-friendliness and natural abundance. The metal tungstate family is an essential group of inorganic materials with applications in many fields because of high oxidation state of the tungsten atom [17–20]. This family of compounds can crystallize in either scheelite or wolframite

* Corresponding author.
E-mail address: kishan@nitk.edu.in (D. Krishna Bhat).

http://dx.doi.org/10.1016/j.jelechem.2017.05.051
Received 30 January 2017; Received in revised form 4 May 2017; Accepted 29 May 2017
Available online 30 May 2017

structure [20]. $ZnWO_4$ has significantly improved the performance in lithium ion batteries, because both zinc and tungsten are electrochemically active metals with respect to lithium metal. Hence, $ZnWO_4$ can be a promising electrode material for electrochemical applications.

In this context, we recently reported the preparation of novel noble metal free graphene based $ZnWO_4/Fe_3O_4$ ternary nanocomposites with excellent efficiency as catalyst for photodegradation of dyes and nitrophenol reductions [21,22]. Inspired by this, we investigated the performance of the catalyst for ORR. The composite shows high activity as electrocatalyst compared to the individual components of the composite. Furthermore, it exhibits high stability and excellent methanol tolerance compared to 20 wt% Pt/C in alkaline medium. This is also the first report on ternary composite $RGO/ZnWO_4/Fe_3O_4$ as a catalyst material for the ORR.

2. Materials and methods

2.1. Materials

Graphite flakes, zinc acetate, iron acetate and Nafion were purchased from Sigma Aldrich. Sodium tungstate, potassium permanganate, potassium hydroxide, ammonia, sulphuric acid, hydrochloric acid, hydrogen peroxide, ethylene glycol and ethanol were purchased from Merck Chemicals Ltd. 20 wt% Pt/C catalyst was purchased from E-Tek. All the chemicals were used without further purification. All solutions were prepared using de-ionized (DI) water.

2.2. Synthesis of $RGO/ZnWO_4/Fe_3O_4$ nanocomposites

GO was synthesized from graphite flakes by using previously reported procedure [22]. $RGO/ZnWO_4/Fe_3O_4$ nanocomposite was synthesized by a one-step microwave irradiation method. GO (24.25 mg) was dispersed in ethylene glycol (48.5 mL) under ultrasonic treatment for about 30 min. 0.05 M (50 mL) of zinc acetate solution and 0.01 M (50 mL) iron acetate solution (in ethanol and water) was added to the above solution. Then 0.05 M (50 mL) sodium tungstate solution was slowly added to the reaction mixture under stirring. Ammonia solution (10 mL) was also slowly added to the above reaction mixture under stirring. The pH of the solution was maintained at 9.0. After 30 min of stirring, the reaction mixture was treated with microwave irradiation at 350 W for 10 min. The blackish precipitate was collected and washed with DI water and ethanol (10%) several times. Finally, the obtained powder was dried in a vacuum oven at 80 °C for 12 h.

2.3. Characterization

The structural and morphological features of the as-synthesized samples were studied using TEM (Tecnai G20) operating at 200 kV and HRTEM (Tecnai) operating at 120 kV, respectively. To determine the crystal structure of the synthesized materials, XRD (Rigaku Corporation, Japan) analysis was performed using nickel-filtered Cu K_α radiation ($\lambda = 0.15406$ nm). The scan rate was set to $2^\circ\ min^{-1}$ for a 2θ range of 5°–70°. The physical properties and elemental composition of the materials were examined using XPS. The XPS analysis was carried out with Multilab 2000 Thermo Scientific (UK) X-ray photoelectron spectrometer. Mg K_α X-ray (1253.6 eV) with 200 W power was used as the exciting source and 10 eV energy pass was used for data collection. The energy analyzer employed was a hemispherical analyzer of 150 mm diameter and 10^{-10} mbar vacuum was maintained during the analysis. Experimental data was curve fitted using Shirley background with a Gaussian and Lorentzian mix product function. Raman spectra were measured by Laser Raman microscope (Renishaw) with a 532.8 nm excitation laser from He-Ne source.

2.4. Electrochemical measurements

Electrochemical experiments were performed using IVIUM instrument in a standard three-electrode cell set up at room temperature (25 ± 1 °C). A glassy carbon (GC), platinum and Ag/AgCl (in saturated KCl solution) served as working, counter and reference electrode. All the potential values reported in this work were referenced to that of reversible hydrogen electrode (RHE), according to the following relation:

$$E_{(RHE)} = E_{Ag/AgCl} + 0.059\,pH + E^{o}{}_{Ag/AgCl,}$$

where, $E^{o}_{Ag/AgCl} = 0.1976$ V at 25 °C and $E_{Ag/AgCl}$ is working potential.

The ORR experiments were carried out using LSV from 1.148 V to 0.148 V using RDE in an O_2 saturated 0.1 M KOH aqueous electrolyte at a scan rate of $10\ mV\ s^{-1}$. The glassy carbon electrode (GCE) was polished successively with 1.0, 0.3 and 0.05 μm alumina slurry followed by thorough sonication in distilled water, absolute ethanol and finally in distilled water for 3 min and used for further electrochemical studies. The working electrode was prepared as follows: 5 mg of the prepared catalyst was dispersed in 1.0 mL water/ethanol (3:1 v/v) solution containing 10 μL Nafion (5 wt%), and the above dispersion was sonicated for 30 min to form a homogeneous catalyst ink. A calculated amount of this ink was then drop cast onto the GCE with the loading controlled at $0.28\ mg\ cm^{-2}$. For comparison, the experiments were also carried out employing the same quantity of RGO, $ZnWO_4$, Fe_3O_4, $RGO/ZnWO_4$, RGO/Fe_3O_4 and 20 wt% Pt/C catalyst being loaded on GCE following the same procedure.

The electron transfer number (n) in the ORR is calculated by Koutecky-Levich (K-L) equation, as below:

$$\frac{1}{j} = \frac{1}{j_k} + \frac{1}{B\sqrt{\omega}}$$

The parameter B is defined as, $B = 0.62n\ FC_o(D_o)^{2/3}\upsilon^{-1/6}$ and $j_k = nFkC_o$, where j is the current density, j_k is the kinetic current density, B is the Levich slope, ω is the electrode rotation speed, n is the number of electrons involved in ORR process per O_2 molecule, C_o is the saturation concentration of oxygen in electrolyte ($1.2 \times 10^{-6}\ mol\ L^{-1}$), D_o is the diffusion coefficient ($1.9 \times 10^{-5}\ cm^2\ s^{-1}$), F is the Faraday constant ($96{,}495\ C\ mol^{-1}$), υ is the kinematic viscosity of solution ($1.0 \times 10^{-2}\ cm^2\ s^{-1}$), k is electron transfer rate constant and ω is the rotation rate in rpm.

The percentage of hydrogen peroxide and the electron transfer number can be determined by the following equations:

$$\%\ -\ H_2O_2 = 200 \times \frac{I_r/N}{I_d + I_r/N}$$

$$n = 4 \times \frac{I_d}{I_d + I_r/N}$$

where I_d is the disk current, I_rI_r is the ring current and N is the current collection efficiency of the Pt ring (0.37) [23]. The Pt-ring electrode was polarized at 0.2 V vs Ag/AgCl for the oxidation of hydrogen peroxide intermediates.

Rotating ring-disc electrode (RRDE) voltammetry was carried out by drop casting the sample on a GC-disc Pt ring electrode. The geometrical surface area of the GCE was used to calculate the current density.

3. Results and discussion

3.1. Morphology studies

The structure and morphological features of the synthesized $RGO/ZnWO_4/Fe_3O_4$ nanocomposite material were investigated by microscopic techniques. Fig. 1a shows the TEM image of $RGO/ZnWO_4/Fe_3O_4$ nanocomposite material in which two dimensional crumpled sheet like RGO morphology decorated with rod shaped $ZnWO_4$ (20 nm–40 nm)

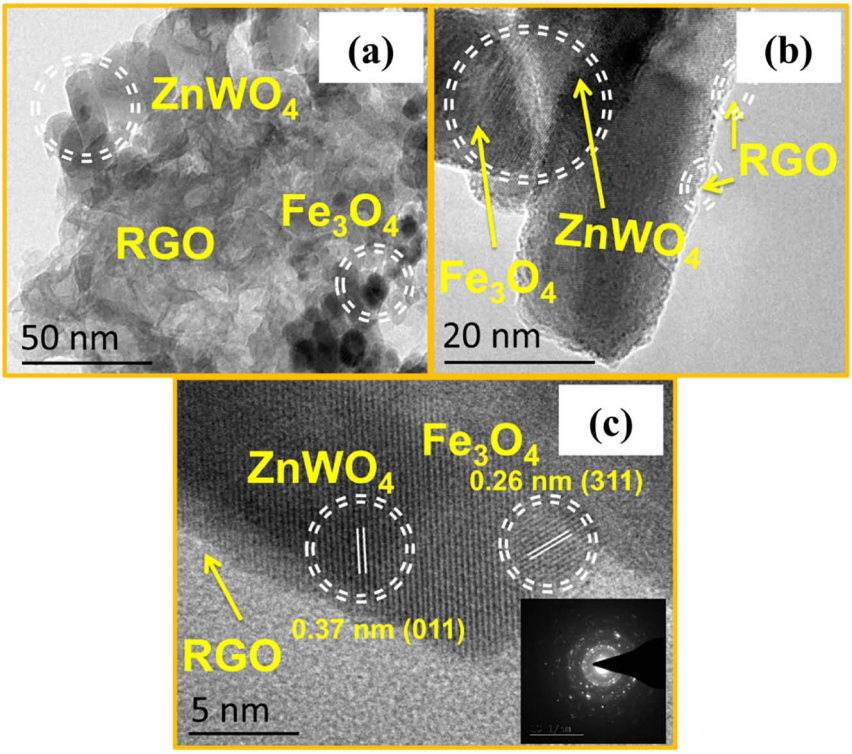

Fig. 1. Microscopy images of RGO/$ZnWO_4$/Fe_3O_4 nanocomposite (a) low magnification TEM, (b) high magnification TEM and (c) HRTEM (inset SAED).

and spherical Fe_3O_4 (10 nm–20 nm) nanoparticles are seen. The magnified image of the same is shown in Fig. 1b. Fig. 1c shows the HRTEM image of RGO/$ZnWO_4$/Fe_3O_4 where the clear interface between $ZnWO_4$ and Fe_3O_4 nanoparticles on the surface of the RGO sheet can be observed. The selected area electron diffraction (SAED) (inset of Fig. 1c) confirms that the $ZnWO_4$ and Fe_3O_4 nanoparticles on RGO sheets are polycrystalline in nature.

3.2. XRD studies

Fig. 2 shows the XRD patterns of the as-prepared RGO, $ZnWO_4$, Fe_3O_4 and RGO/$ZnWO_4$/Fe_3O_4. The diffraction peak at 22.6° and 42.6° are indexed to the (002) and (100) planes of RGO sheets. The typical diffraction peaks at 18.7°, 23.6°, 24.3°, 30.4° and 36.3° were ascribed to the (100), (011), (110), (111) and (-111) crystal planes of $ZnWO_4$, well matched with JCPDS data [File no. 15-0774]. The diffraction peaks at 30.3°, 35.6°, 43.4°, 53.7°, 57.3° and 62.9° can be indexed to the (220), (311), (400), (422), (511) and (440) planes of Fe_3O_4 crystal and are in good agreement with JCPDS data [File no. 19-0629]. In ternary composites of RGO/$ZnWO_4$/Fe_3O_4, no carbon diffraction peak for RGO was detected in the XRD patterns, which may be due to the small amount of RGO in the composite samples [22]. However, the existence of RGO in the composites was confirmed by TEM, Raman and XPS analysis (given in later section).

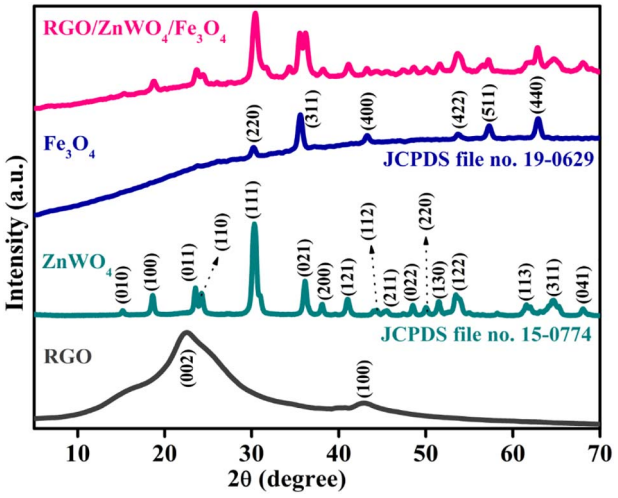

Fig. 2. XRD spectra of synthesized RGO, $ZnWO_4$, Fe_3O_4 and RGO/$ZnWO_4$/Fe_3O_4 nanocomposite.

3.3. XPS studies

XPS spectra of the samples were measured to get further information on the chemical states of ions in the composites formed (Fig. 3). Binding energy was calibrated by taking the C 1s peak (284.8 eV) as a reference. Fig. 3a shows the general survey spectra of the as-prepared RGO/$ZnWO_4$/Fe_3O_4 composite which displays that the surfaces contain C, Zn, W and Fe. Fig. 3b shows the C 1s spectra region, which could be deconvoluted into four peaks with binding energies of 284.8 eV, 286.6 eV, 288.1 eV and 290.1 eV. These peaks are assigned to the bonds, C–C/C=C in the aromatic ring of sp^2, C–O, C=O and O–C=O in the oxygenated functional groups respectively. These results indicate that GO has been well deoxygenated to form graphene sheets [24]. Fig. 3c shows the O 1s spectra region, which could be deconvoluted into three peaks of values, 529.9 eV, 531.6 eV and 533 eV corresponding to Fe–O, W–O–W and O–H bonds of the surface adsorbed water respectively [22]. Fig. 3d shows the Zn 2p region, consisting of two peaks at 1019.1 eV and 1041.9 eV, which are assigned to the Zn $2p_{3/2}$ and Zn $2p_{1/2}$ state, respectively [22]. Fig. 4e shows the W 4f region, with two peaks at 36.8 eV and 38.8 eV being assigned to W $4f_{7/2}$ and W $4f_{5/2}$, respectively. These results match with those reported previously [21,22]. Fig. 4f shows binding energies of Fe 2p region. Two photoelectron peaks at 709.2 eV and 723.5 eV correspond to Fe $2p_{3/2}$ and Fe $2p_{1/2}$ states respectively [25]. Overall the results confirm that the component particles, $ZnWO_4$ and Fe_3O_4 are well incorporated into the RGO matrix.

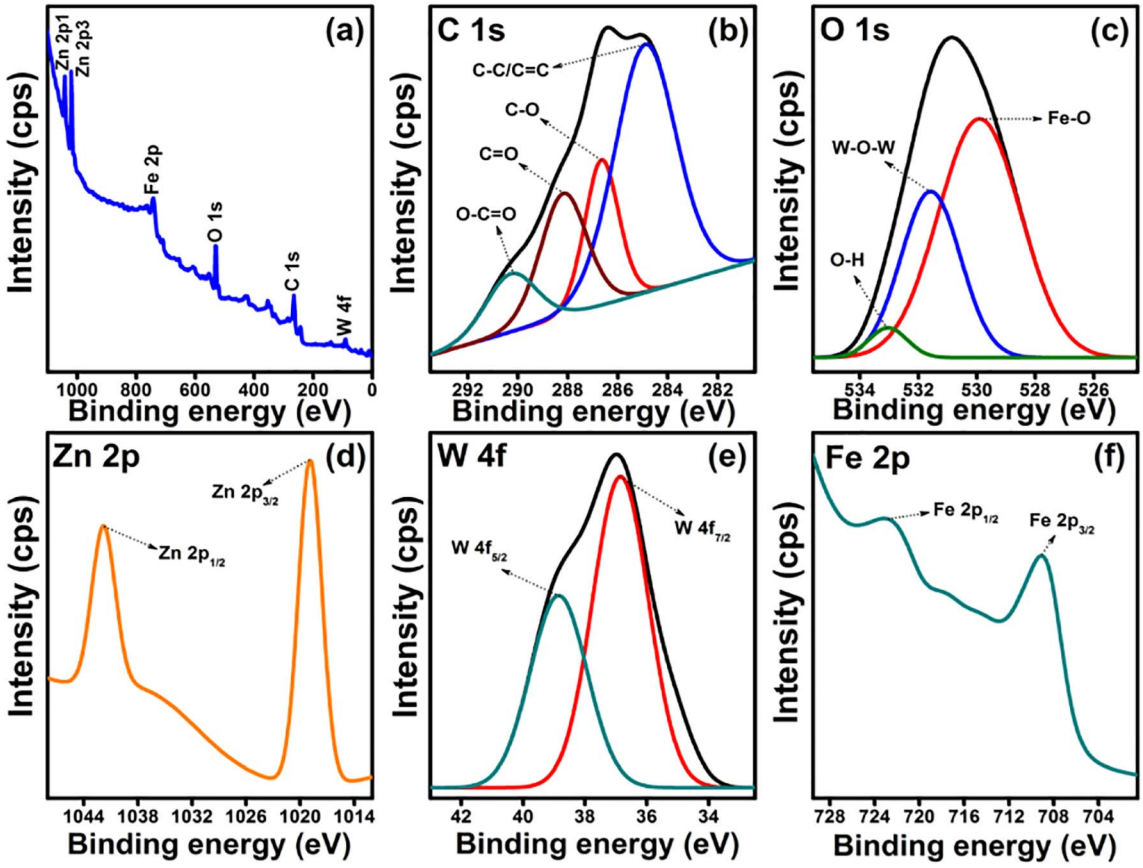

Fig. 3. XPS spectra of RGO/$ZnWO_4$/Fe_3O_4 nanocomposites (a) survey, (b) C 1s, (c) O 1 s, (d) Zn 2p, (e) W 4f and (e) Fe 2p.

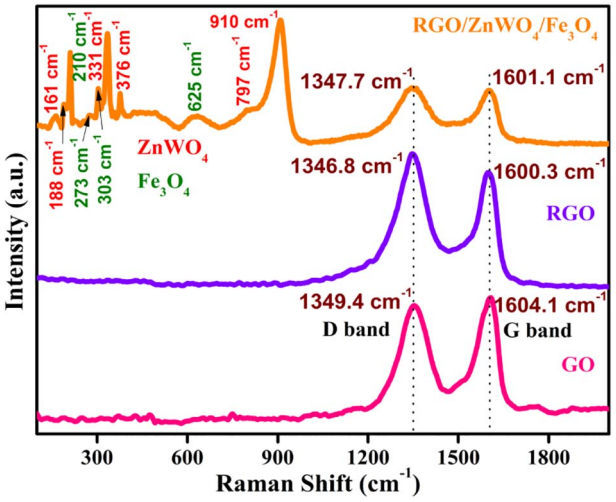

Fig. 4. Raman spectra of GO, RGO and RGO/$ZnWO_4$/Fe_3O_4 nanocomposites.

3.4. Raman studies

The obtained Raman spectra of RGO/$ZnWO_4$/Fe_3O_4 composite samples are shown in Fig. 4. Four peaks around 210 cm^{-1}, 273 cm^{-1}, 303 cm^{-1} and 625 cm^{-1} correspond to the characteristic Raman mode of the magnetite phase of Fe_3O_4. Six peaks around 161 cm^{-1}, 188 cm^{-1}, 331 cm^{-1}, 376 cm^{-1}, 797 cm^{-1} and 910 cm^{-1} correspond to the characteristic Raman mode of the monoclinic phase of $ZnWO_4$. Two peaks around 1347.7 cm^{-1} and 1601.1 cm^{-1} correspond to the plane vibrations of sp^3 defects in carbon (D band) and sp^2 bonds of carbons (G band) of RGO sheets [26]. D to G band peak intensity ratio, I_D/I_G, is generally used to confirm the degree of defects of the carbon nanomaterial. The calculated intensity ratio of RGO and RGO/$ZnWO_4$/Fe_3O_4 (I_D/I_G = 1.10 and 1.03, respectively) is higher than that of GO (I_D/I_G = 0.98), indicating the introduction of defects, the removal of oxygenated functional groups during the reduction of GO into RGO sheets. The lower I_D/I_G of RGO/$ZnWO_4$/Fe_3O_4 than that of RGO may be due to the presence of $ZnWO_4$ and Fe_3O_4 nanoparticles on the RGO sheets. Also, the broad D band and G band with weak intensity can be ascribed to the coverage of $ZnWO_4$ and Fe_3O_4 nanoparticles on the RGO sheets. Above mentioned results confirm that the $ZnWO_4$, Fe_3O_4 have been successfully anchored to the RGO sheets and match well with the previous reports [21,22].

3.5. Electrocatalytic activity towards ORR

The LSV method was employed to study the electrochemical activity of RGO/$ZnWO_4$/Fe_3O_4 catalyst material towards ORR. The LSVs were first measured in N_2 and then in O_2 saturated 0.1 M KOH aqueous electrolyte at a scan rate of 10 mV s^{-1}. As shown in Fig. 5a, under N_2 atmosphere, no anodic or cathodic peaks were observed, only a straight line of the cathodic current for RGO/$ZnWO_4$/Fe_3O_4 nanocomposite modified electrode is observed. However, after O_2 is introduced, a profound cathodic current voltammetric curve is observed with an onset potential of 0.965 V vs RHE and the same for 20 wt% Pt/C commercial catalyst is also shown in Fig. 5b for the sake of comparison.

To evaluate the electrocatalytic activity of RGO/$ZnWO_4$/Fe_3O_4 catalyst further, RDE measurements of different samples are compared. Fig. 5c shows the polarization curves for RGO, $ZnWO_4$, Fe_3O_4, RGO/$ZnWO_4$, RGO/Fe_3O_4, RGO/$ZnWO_4$/Fe_3O_4 and 20 wt% Pt/C materials at a scan rate of 10 mV s^{-1} with a rotation rate of 1600 rpm. From Fig. 5c, it is clearly seen that the sample (RGO) prepared without any transition metal showed the lowest ORR activity in terms of current density and

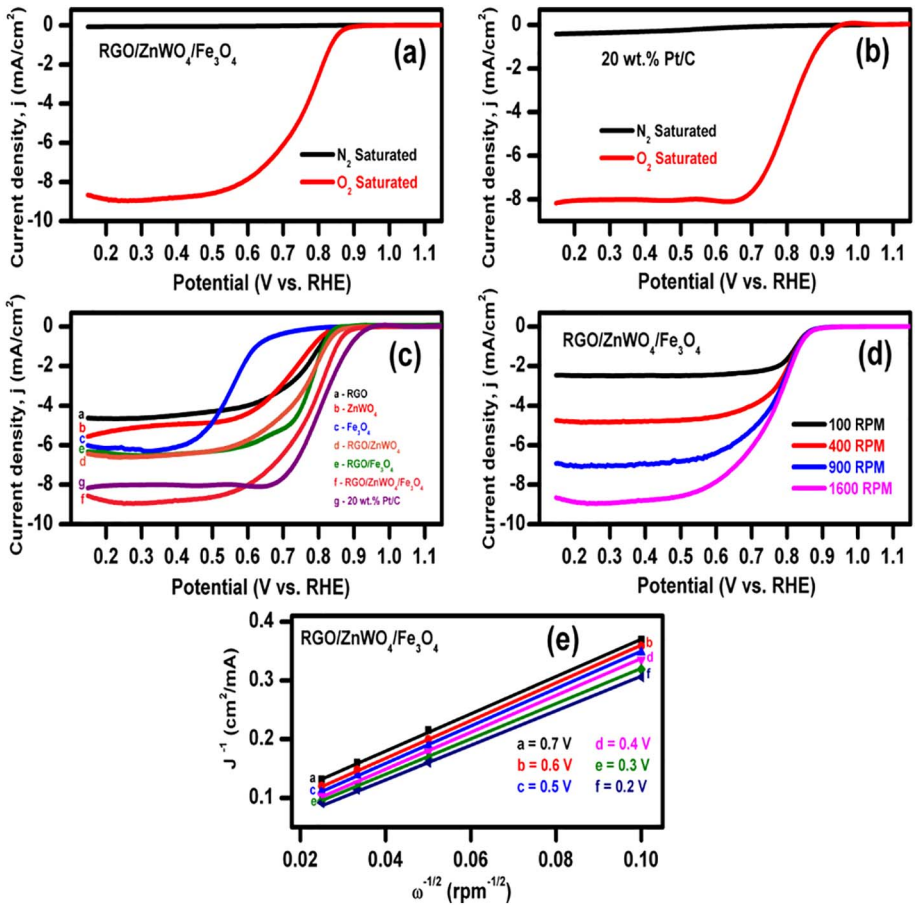

Fig. 5. LSV curves for (a) RGO/$ZnWO_4$/Fe_3O_4, (b) Pt/C catalysts, (c) various electrocatalysts on RDE O_2-saturated 0.1 M KOH aqueous solution at 1600 rpm, (d) RGO/$ZnWO_4$/Fe_3O_4 on RDE O_2-saturated 0.1 M KOH aqueous solution at various rotation rates; (e) K-L plots at different potentials of RGO/$ZnWO_4$/Fe_3O_4.

onset potential. Transition metal oxides Fe_3O_4 and $ZnWO_4$ alone also exhibited meagre electrochemical activity towards ORR in terms of onset potential. However, after compositing with RGO and Fe_3O_4, the ORR onset potential for the catalyst material shifts positively for about 20 mV with an enhanced current density. The voltammetric current density for ORR on RGO/$ZnWO_4$/Fe_3O_4 (8.9 mA cm^{-2}) is two times more than that of $ZnWO_4$ (4.5 mA cm^{-2}). The onset potentials follow the trend: 20 wt% Pt/C > RGO/$ZnWO_4$/Fe_3O_4 > RGO/$ZnWO_4$ > RGO/Fe_3O_4 > RGO > $ZnWO_4$ > Fe_3O_4. The lowest onset potential for ORR at RGO/$ZnWO_4$/Fe_3O_4 is measured to be 0.965 V which is more positive than RGO, $ZnWO_4$, Fe_3O_4, RGO/$ZnWO_4$ and RGO/Fe_3O_4. In addition to this RGO/$ZnWO_4$/Fe_3O_4 material has also showed higher current density than other synthesized materials as reported in the literature [27].

The fact that the performance of ternary nanocomposite is much better than the individual binary components namely, the RGO/$ZnWO_4$ and RGO/Fe_3O_4 very clearly suggests that the combination is producing the observed high performance of the nanocomposite catalyst through a synergistic mechanism. This may be due to the availability of an effective surface area with activated adsorption sites provided by the combination of $ZnWO_4$ and Fe_3O_4 for the reduction reaction. The process is further facilitated by the high conductivity matrix of RGO. The results also establish the importance of the synergistic effects in the development of novel high-performance catalyst materials as is evident from the enhanced electrocatalytic performance of RGO/$ZnWO_4$/Fe_3O_4 nanocomposite towards ORR imparted by the doping of trace amount of Fe_3O_4 into the RGO-$ZnWO_4$ matrix.

To further understand the ORR mechanism, kinetic parameters of RGO/$ZnWO_4$/Fe_3O_4 catalyst were measured. Fig. 5d shows the LSV curves of RGO/$ZnWO_4$/Fe_3O_4 samples recorded in O_2 saturated 0.1 M KOH electrolyte at different rotation rates (100, 400, 900 and 1600 rpm). It is observed that the current density increased with rotation rate. For comparison, other synthesized materials are also examined under the same conditions (Fig. 6). The polarization curves and the corresponding Koutecky-Levich (K-L) plot in the potential range from 0.2 V to 0.7 V is shown in Fig. 5e. According to K-L plot, j^{-1} vs $\omega^{-1/2}$ should give parallel straight lines at different applied potentials [28]. The K-L plots (Fig. 5e) of RGO/$ZnWO_4$/Fe_3O_4 catalyst are linear and show relatively consistent slope within this potential range suggesting first order reaction kinetics with respect to the concentration of dissolved O_2 in the solution. Further, the plots do not pass through the origin, demonstrating that the mixed kinetic-diffusion-controlled mechanism is in operation for the process [29]. For comparison, the other materials are examined under the same conditions (Fig. 7). There are two characteristic pathways for the reduction of molecular O_2 under basic condition: (a) reduction of O_2 to OH^- (via $4e^-$ process) and (b) reduction of O_2 to HO_2^- HO_2^- (via $2e^-$ process) followed by further reduction of HO_2^- to OH^- or by desorption of HO_2^- into solution [17]. The calculated electron transfer numbers for RGO/$ZnWO_4$/Fe_3O_4 at different potentials are near to 3.8 which suggest that the composite material favors a greater selectivity via $4e^-$ pathway towards ORR. Thus, the probable ORR mechanism is given as follows:

$$O_2 + 2H_2O + 4e^- \rightarrow 4OH^-$$

As can be seen from the literature, many attempts have been made to develop alternative catalysts, to replace or to reduce the Pt content in catalysts for ORR. To the best of our knowledge, the performances of these alternative catalysts for ORR are still unsatisfactory and rarely exceed the performance of Pt/C. Although the heteroatom-doped graphene, graphene composites, graphene with metal oxide composites

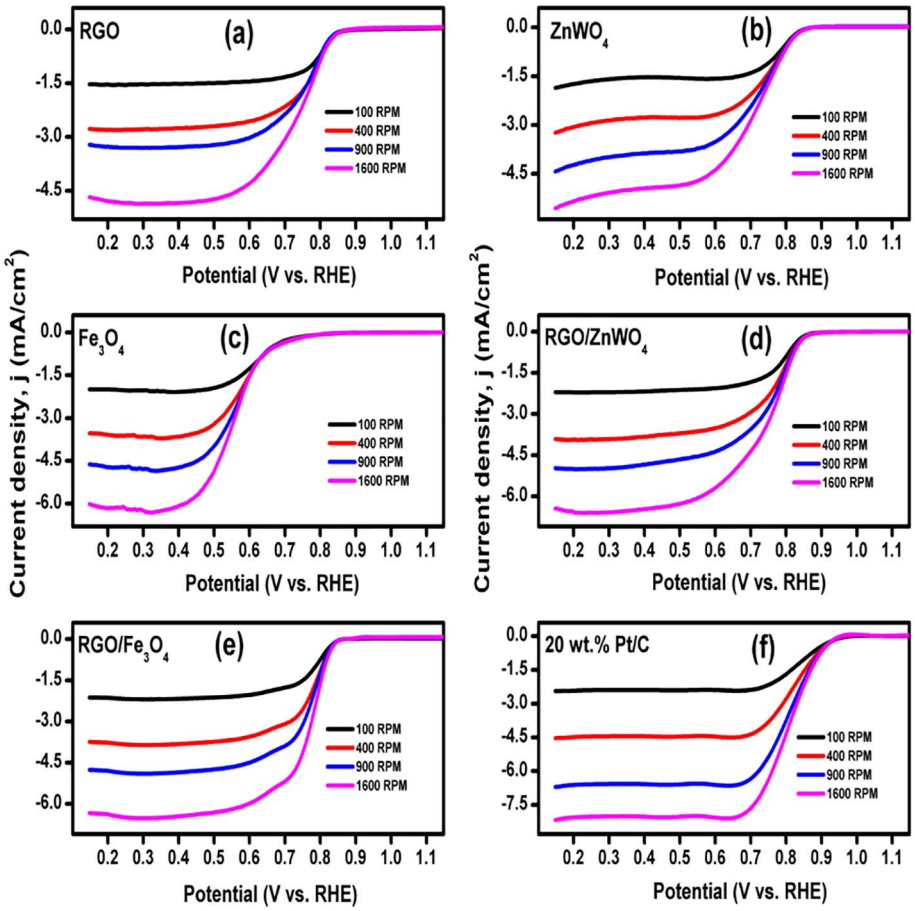

Fig. 6. LSV obtained for various electrocatalysts on RDE electrode O_2-saturated 0.1 M KOH aqueous solution at various rotation rates with scan rate of 10 mV s^{-1}.

and transition metal atom doped graphene materials have been proved to have excellent capacity for ORR, our results are comparable and rather better than these materials [30–34] and remarkably higher than previously reported graphene based materials. Thus, this RGO/$ZnWO_4$/Fe_3O_4 catalyst could be an ideal candidate as an alternative to Pt catalysts, offering a new perspective for a less expensive cathode without compromising the performance.

To elucidate the ORR kinetics of the RGO/$ZnWO_4$/Fe_3O_4 sample further, RRDE measurements are conducted at a rotation speed of 1600 rpm in O_2 saturated 0.1 M KOH. In this technique, the yield of H_2O_2 is exactly determined from the ring and disk currents through the ORR [23]. The LSV obtained from this test is shown in Fig. 8.

The detected hydrogen peroxide yield for RGO/$ZnWO_4$/Fe_3O_4 nanocomposites was 1.8%, which is close to that of commercial Pt/C (2.5–6.1%) implying that the primary product is OH^- in the ORR process. Hence from this observation, it is evident that the ORR process on the present catalyst proceeds preferentially via a $4e^-$ pathway. Furthermore, the kinetic current is readily quantified from the ORR polarization curves by using the K-L equation, from which the mass activities are calculated by normalizing the kinetic current [35]. This mass activity is regarded as the essential feature for comparing the catalytic activity of different catalysts, because it is associated with the intrinsic activity of the catalyst. Accordingly, comparison of the mass activity between series of synthesized materials and commercial Pt/C at 0.6 V is given in Fig. 9. The result shows that RGO/$ZnWO_4$/Fe_3O_4 exhibited a slightly better ORR performance compared to commercial Pt/C.

To estimate the properties of a novel electrocatalyst towards ORR, the methanol tolerance to crossover effect also needs to be considered [14]. As shown in Fig. 10a, LSV curves of RGO/$ZnWO_4$/Fe_3O_4 were examined for ORR in the absence and in the presence of high concentration of methanol (2 M) in O_2 saturated 0.1 M KOH electrolyte solution. The LSV response of RGO/$ZnWO_4$/Fe_3O_4 essentially demonstrates a negligible change in its activity after the addition of methanol, which signposts that the RGO/$ZnWO_4$/Fe_3O_4 has an extraordinary tolerance to crossover effect against methanol. It is fascinating to note that the presence of methanol does not evidently alter the electrocatalytic performance of the nanocomposite towards ORR. In contrast, there is a clear decrease in the ORR performance of commercial 20 wt% Pt/C, because of the competitive reaction between ORR and methanol oxidation (inset of Fig. 10a). Thus, the result suggests that RGO/$ZnWO_4$/Fe_3O_4 catalyst has much better resistance towards methanol crossover effect and hints at the usefulness of RGO/$ZnWO_4$/Fe_3O_4 nanocomposite as a methanol tolerant ORR catalyst in alkaline fuel cell configuration that provides an economical advantage over the state-of-the-art conventional 20 wt% Pt/C materials.

Another primary concern is the stability of catalysts. The stability test of LSV curves recorded for RGO/$ZnWO_4$/Fe_3O_4 in O_2 saturated 0.1 M KOH electrolyte before and after 2000 cycles between 1.148 V to 0.148 V at 1600 rpm is shown in Fig. 10b. The polarization curve shows about 5 mV negative shift in the onset potential after 2000 cycles, indicating the high stability of the RGO/$ZnWO_4$/Fe_3O_4 catalyst. Whereas, in the case of 20 wt% Pt/C (inset of Fig. 10b) the onset potential is shifted to around 40 mV after 2000 cycles. This evidence clearly shows that the RGO/$ZnWO_4$/Fe_3O_4 is more stable than 20 wt% Pt/C, for fuel cell applications. Further, we have also carried out TEM and EDX analysis of RGO/$ZnWO_4$/Fe_3O_4 catalyst after the reduction experiment. As can be observed from the images, there are no obvious changes in the morphology or the chemical composition (Fig. 11). Based on these observations, the present RGO/$ZnWO_4$/Fe_3O_4 catalyst is expected to offer an intense activity towards ORR.

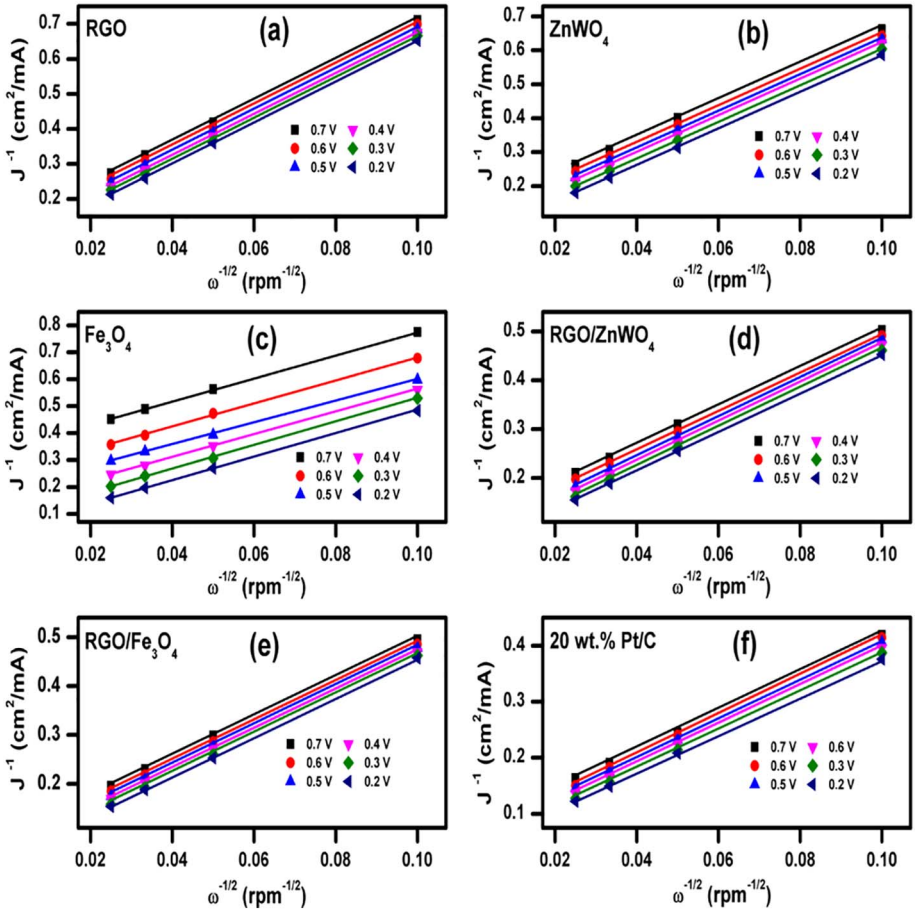

Fig. 7. K-L plots obtained for various electrocatalysts at different potentials.

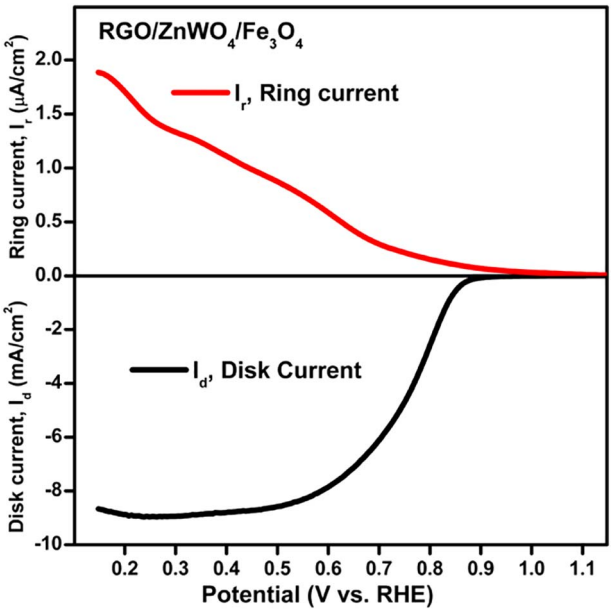

Fig. 8. LSV of RRDE test on $RGO/ZnWO_4/Fe_3O_4$ in O_2 saturated 0.1 M KOH aqueous solution at 1600 rpm with a scan rate of 10 mV s^{-1}.

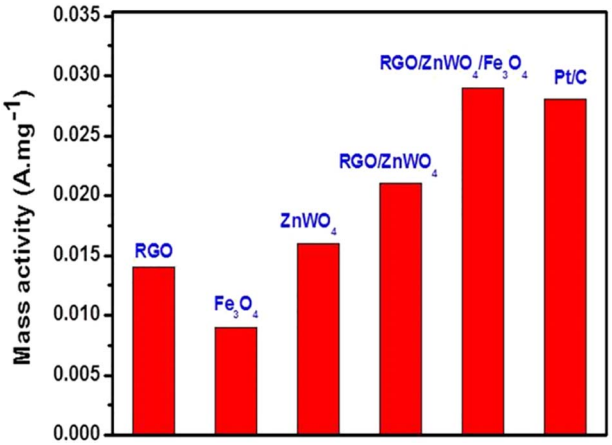

Fig. 9. Comparison of the mass activities for different catalyst materials measured at 0.6 V vs RHE. All the measurements were performed in O_2 saturated 0.1 M KOH at a rotation rate of 1600 rpm and scan rate of 10 mV s^{-1}.

4. Conclusions

In this study, a scalable, facile, template-free and rapid technique for the synthesis of electrocatalysts using microwave irradiation method is developed. The catalysts are characterized by XRD, XPS, TEM, HRTEM and Raman measurements. The $RGO/ZnWO_4/Fe_3O_4$ material has an outstanding electrocatalytic activity for the ORR in alkaline solution. It is seen that compared to RGO, $ZnWO_4$, RGO/Fe_3O_4, $RGO/ZnWO_4$ and commercial 20 wt% Pt/C catalyst, the $RGO/ZnWO_4/Fe_3O_4$ nanocomposite shows higher electrocatalytic activity. The RDE and RRDE experiments revealed that mechanism of ORR on this nanocomposite follows a four-electron pathway. In addition to high ORR activity, the $RGO/ZnWO_4/Fe_3O_4$ nanocomposite catalyst also has high stability, recyclability and excellent tolerance towards methanol. Hence $RGO/ZnWO_4/Fe_3O_4$ composite is expected to be a promising, low-cost, highly active material in fuel cell manufacturing.

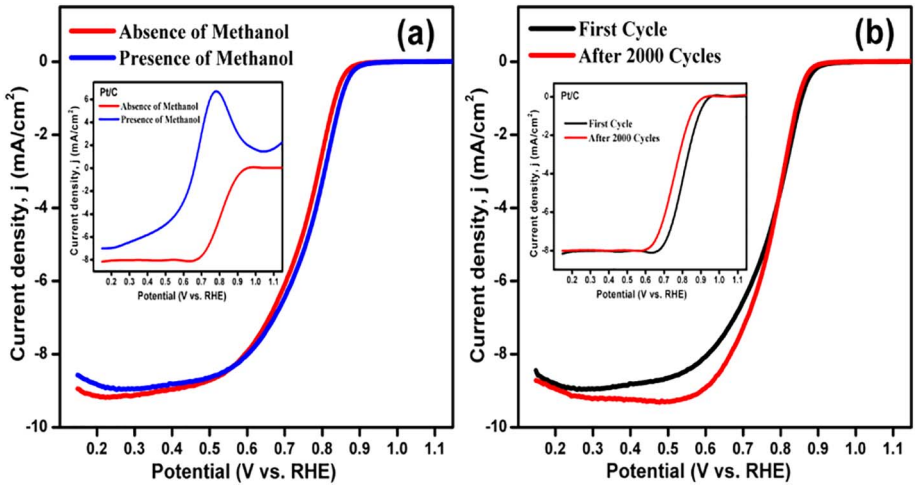

Fig. 10. (a) LSVs of Methanol tolerance test performed on RGO/$ZnWO_4$/Fe_3O_4 in O_2 saturated 0.1 M KOH containing 2 M methanol, (Inset shows Methanol tolerance test of 20 wt% Pt/C catalyst), (b) LSVs of stability analysis performed on RGO/$ZnWO_4$/Fe_3O_4 in O_2 saturated 0.1 M KOH aqueous solution before and after 2000 cycles (Inset shows stability test of 20 wt% Pt/C).

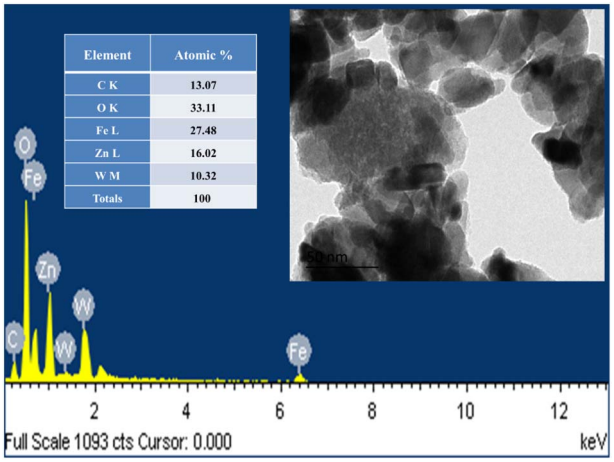

Fig. 11. EDX spectrum of RGO/$ZnWO_4$/Fe_3O_4 nanocomposite after stability test (inset TEM image, the scale shows 50 nm length).

Acknowledgement

M.J.S.M. is grateful to National Institute of Technology Karnataka Surathkal, for the award of a research fellowship.

References

[1] B.C. Steele, A. Heinzel, Materials for fuel-cell technologies, Nature 414 (2001) 345–352.
[2] Y.A. Zehtab, H. Fei, R. Ye, G. Wang, J. Tour, U. Sundararaj, Boron/nitrogen co-doped helically unzipped multiwalled carbon nanotubes as efficient electrocatalyst for oxygen reduction, ACS Appl. Mater. Interfaces 7 (2015) 7786–7794.
[3] M.K. Debe, Electrocatalyst approaches and challenges for automotive fuel cells, Nature 486 (2012) 43–51.
[4] H. Li, W. Kang, L. Wang, Q. Yue, S. Xu, H. Wang, J. Liu, Synthesis of three-dimensional flowerlike nitrogen-doped carbons by a copyrolysis route and the effect of nitrogen species on the electrocatalytic activity in oxygen reduction reaction, Carbon 54 (2013) 249–257.
[5] V.R. Stamenkovic, B.S. Mun, M. Arenz, K.J. Mayrhofer, C.A. Lucas, G. Wang, P.N. Ross, N.M. Markovic, Trends in electrocatalysis on extended and nanoscale Pt-bimetallic alloy surfaces, Nat. Mater. 6 (2007) 241–247.
[6] Y. Liang, Y. Li, H. Wang, J. Zhou, J. Wang, T. Regier, H. Dai, Co_3O_4 nanocrystals on graphene as a synergistic catalyst for oxygen reduction reaction, Nat. Mater. 10 (2011) 780–786.
[7] B. Subramanya, D.K. Bhat, S.U. Shenoy, Y. Ullal, A.C. Hegde, Novel Fe-Ni-Graphene composite electrode for hydrogen production, Int. J. Hydrog. Energy 40 (2015) 10453–10462.
[8] B. Subramanya, Y. Ullal, S.U. Shenoy, D.K. Bhat, A.C. Hegde, Novel Co-Ni-graphene composite electrodes for hydrogen production, RSC Adv. 5 (2015) 47398–47407.
[9] Y.N. Sudhakar, M. Selva kumar, D.K. Bhat, S. Senthilkumar, Reduced graphene oxide derived from used cell graphite, and its green fabrication as eco-friendly supercapacitor, RSC Adv. 4 (2014) 60039–60051.
[10] X. Huang, X. Qi, F. Boeya, H. Zhang, Graphene-based composites, Chem. Soc. Rev. 41 (2012) 666–686.
[11] B. Subramanya, D.K. Bhat, Novel eco-friendly synthesis of graphene directly from graphite using TEMPO and study of its electrochemical properties, J. Power Sources 275 (2015) 90–98.
[12] B. Subramanya, D.K. Bhat, Novel one-pot green synthesis of graphene in aqueous medium under microwave irradiation using regenerative catalyst and study of its electrochemical properties, New J. Chem. 39 (2014) 420–430.
[13] H. Peng, Z. Mo, S. Liao, H. Liang, L. Yang, F. Luo, H. Song, Y. Zhong, B. Zhang, High performance Fe- and N-doped carbon catalyst with graphene structure for oxygen reduction, Sci. Rep. 3 (2013) 1–7.
[14] Q. Dong, X. Zhuang, Z. Li, B. Li, B. Fang, C. Yang, H. Xie, F. Zhang, X. Feng, Efficient approach to iron/nitrogen co-doped graphene materials as efficient electrochemical catalysts for the oxygen reduction reaction, J. Mater. Chem. A 3 (2015) 7767–7772.
[15] D.K. Bhat, Facile synthesis of ZnO nanorods by microwave irradiation of zinc-hydrazine hydrate complex, Nanoscale Res. Lett. 3 (2008) 31–35.
[16] T. Hisatomi, J. Kubota, K. Domen, Recent advances in semiconductors for photocatalytic and photoelectrochemical water splitting, Chem. Soc. Rev. 43 (2014) 7520–7535.
[17] Y. Lu, Y. Jiang, X. Gao, X. Wang, W. Chen, Strongly coupled Pd nanotetrahedron/tungsten oxide nanosheet hybrids with enhanced catalytic activity and stability as oxygen reduction electrocatalysts, J. Am. Chem. Soc. 136 (2014) 11687–11697.
[18] M.M.J. Sadiq, D.K. Bhat, Novel $ZnWO_4$/RGO nanocomposite as high performance photocatalyst, AIMS Mater. Sci. 4 (2017) 158–171.
[19] M.M.J. Sadiq, U.S. Shenoy, D.K. Bhat, High performance bifunctional catalytic activity of novel zinc tungstate - reduced graphene oxide nanocomposite, Adv. Sci. Eng. Med. 9 (2017) 115–121.
[20] T. Montini, V. Gombac, A. Hameed, L. Felisari, G. Adami, P. Fornasiero, Synthesis, characterization and photocatalytic performance of transition metal tungstates, Chem. Phys. Lett. 498 (2010) 113–119.
[21] M.M.J. Sadiq, D.K. Bhat, Novel RGO-$ZnWO_4$-Fe_3O_4 nanocomposite as an efficient catalyst for rapid reduction of 4-nitrophenol to 4-aminophenol, Ind. Eng. Chem. Res. 55 (2016) 7267–7272.
[22] M.M.J. Sadiq, U.S. Shenoy, D.K. Bhat, Novel RGO-$ZnWO_4$-Fe_3O_4 nanocomposite as high performance visible light photocatalyst, RSC Adv. 6 (2016) 61821–61829.
[23] W. Wang, J. Geng, L. Kuai, M. Li, B. Geng, Porous Mn_2O_3: a low-cost electrocatalyst for oxygen reduction reaction in alkaline media with comparable activity to Pt/C, Chem. Eur. J. 22 (2016) 9909–9913.
[24] M.M.J. Sadiq, D.K. Bhat, A facile microwave approach to synthesize RGO-$BaWO_4$ composites for high performance visible light induced photocatalytic degradation of dyes, AIMS Mater. Sci. 4 (2017) 487–502.
[25] M.M.J. Sadiq, U.S. Shenoy, D.K. Bhat, Enhanced photocatalytic performance of N-doped RGO-$FeWO_4$/Fe_3O_4 ternary nanocomposite in environmental applications, Mat. Today. Chem. 4 (2017) 133–141.
[26] D. Graf, F. Molitor, K. Ensslin, C. Stampfer, A. Jungen, C. Hierold, L. Wirtz, Spatially resolved Raman spectroscopy of single-and few-layer graphene, Nano Lett. 7 (2007) 238–242.
[27] S. Liu, Y. Dong, C. Zhao, Z. Zhao, C. Yu, Z. Wang, J. Qiu, Nitrogen-rich carbon coupled multifunctional metal oxide/graphene nanohybrids for long-life lithium storage and efficient oxygen reduction, Nano Energy 12 (2015) 578–587.
[28] S. Mutyala, J. Mathiyarasu, A. Mulchandani, Methanol tolerant, high performance, noble metal free electrocatalyst developed from polyaniline and ferric chloride for the oxygen reduction reaction, RSC Adv. 5 (2015) 92648–92655.
[29] P. Li, X. Zhao, C.J. Jia, H. Sun, L. Sun, X. Cheng, L. Liu, W. Fan, $ZnWO_4$/BiOI heterostructures with highly efficient visible light photocatalytic activity: the case of interface lattice and energy level match, J. Mater. Chem. A 1 (2013) 3421–3429.

[30] W. Xia, A. Mahmood, Z. Liang, R. Zou, S. Guo, Earth-abundant nanomaterials for oxygen reduction, Angew. Chem. Int. Ed. 55 (2016) 2650–2676.
[31] M. Shao, Q. Chang, J.P. Dodelet, R. Chen, Recent advances in electrocatalysts for oxygen reduction reaction, Chem. Rev. 116 (2016) 3594–3657.
[32] L. Dai, Y. Xue, L. Qu, H.K. Choi, J.B. Baek, Metal-free catalysts for oxygen reduction reaction, Chem. Rev. 115 (2015) 4823–4892.
[33] J. Liang, M. Hassan, D. Zhu, L. Guo, X. Bo, Cobalt nanoparticles/nitrogen-doped graphene with high nitrogen doping efficiency as noble metal-free electrocatalysts for oxygen reduction reaction, J. Colloid Interface Sci. 490 (2017) 576–586.
[34] Z.S. Wu, S. Yang, Y. Sun, K. Parvez, X. Feng, K. Müllen, 3D nitrogen-doped graphene aerogel-supported Fe_3O_4 nanoparticles as efficient electrocatalysts for the oxygen reduction reaction, J. Am. Chem. Soc. 134 (2012) 9082–9085.
[35] I. Vincent, D. Bessarabov, Electrochemical characterization and oxygen reduction kinetics of Cu-incorporated cobalt oxide catalyst, Int. J. Electrochem. Sci. 11 (2016) 8002–8015.